FINAL REPORT: Potential Field Surveys, Analyses, and Interpretation for Cornell's Earth Source Heat Project

Franklin G. Horowitz*

*Horowitz Consulting, Freeville, NY 13068, USA; frank@horow.net

8-February–2019

Contents

1 Introduction

This work was contracted to look for geological structures that might be proximal to the proposed drilling sites for Cornell University's Earth Source Heat (ESH) project. I used geophysical gravity and magnetic (collectively: potential field or PF) surveys as the underlying data from which I primarily formed my interpretations.

PF surveys offer a relatively low-cost means of identifying underground geological structures in an area of interest. While they certainly can not attain the resolution available from seismic reflection surveys, their low-cost affords a method of covering a much larger map area of interest than would be economical via 2D or 3D reflection seismic surveys.

Here, I report on results and interpretations derived from two independent PF surveys. First, during July 2018 – with the help of field assistants Ming Khan, Emily Boedo, Samantha Moruzzi, and Ole Gustafson – a gravity survey was performed in the region shown in Figure 1 using a rented Scintrex CG5 gravity meter. The region of gravity coverage is shown by the outline of light brown circles and blue features in the figure. Second, a commercial aeromagnetic survey – flown on speculation during exploration activity for the Trenton-Black River gas play in 1999 – was purchased for Tompkins county from geophysical service company EDCON-PRJ. The coverage region is evident via the network of light red lines and green features in the figure.

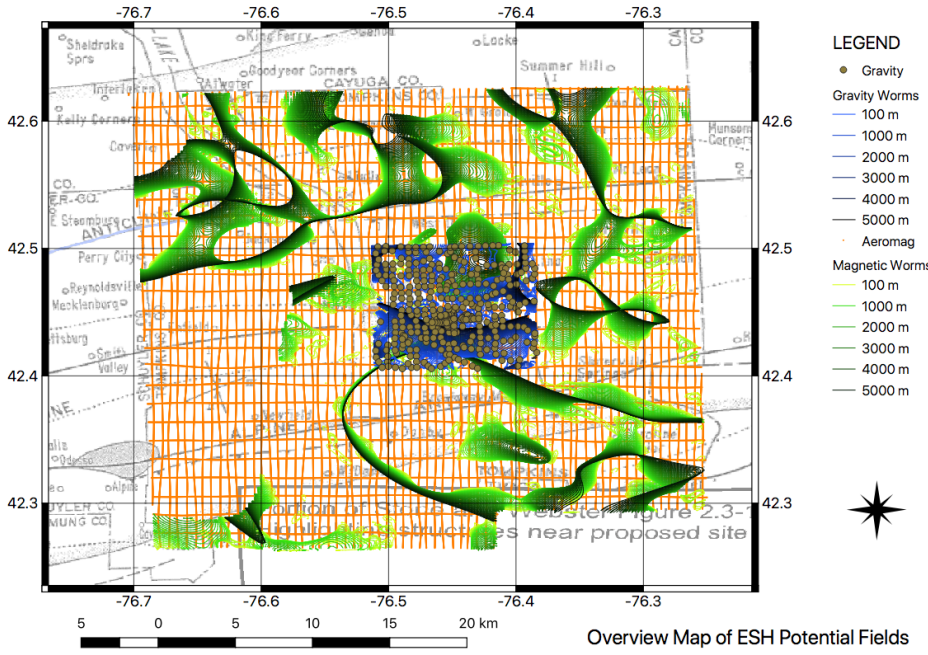

Figure 1: An overview of the sampling locations for both the gravity survey (brown filled circles) and aeromagnetic survey (light red lines) superposed over a generalized geological map of the region (Stone & Webster Engineering Corporation et al., 1978, figure 2.3-1). The green and blue curves are magnetic and gravity multi-scale edges respectively, and will be described in the following sections.

2 Methods 1: Gravity Measurements and Data Reductions

By convention, a gravity survey estimates spatial anomalies in the Earth's gravity accelerations at a nominal elevation of "sea level" – or more precisely its approximation at the height of a specified ellipsoid. The anomalies are ascribed to variations in the mass densities of the rocks underneath the survey's footprint. Once the anomalies are estimated, they are subjected to various techniques in order to interpret the underlying geological structures. This section describes the measurements and data reductions, leaving the analysis technique and interpretation for later sections.

A Scintrex CG5 relative gravity meter was rented during July 2018 for the month-long duration of the survey. Such meters have a manufacturer quoted repeatability of $\pm 5\ \mu Gal$ in the lab. This report will commonly use a traditional gravity measurement unit of milliGals and multiples thereof – Gals being a cgs unit for acceleration named after Galileo. However, for reference the conversion factor to SI units is $1\ Gal = 10^{-2} m/s^2$. Hence 5 μGal is equivalent to $5 \times 10^{-8} m/s^2$. Compared to the full order of magnitude of $g \approx 10 m/s^2$, the CG5 hence has a sensitivity of around 5 ppb – somewhat remarkable for a field portable mechanical instrument.

The CG5 samples gravity at 6Hz reporting the average and standard deviation of the time series at each station. During this survey, the CG5 was configured to read for 60 seconds, yielding a nominal 360 gravity measurements at each station. The on-board "seismic filter" was enabled, which during periods of high noise results in the CG5 rejecting *outlier* readings via an algorithm proprietary to Scintrex. This setting commonly rejected a small number of the 360 samples at each station. In the field, other noise sources such as wind, traffic, moving water etc. also causes measurement outliers. I subjectively re-measured a station whenever I judged the standard deviation reported by the meter to be "too high".

I used two of the CG5's on-board aids to gravity data reduction. First, I used an approximate drift correction – intended to account for a time-varying systematic stretching of the CG5's quartz spring – based on an overnight calibration run at the beginning of the survey. Second I used an on-board correction for tidal effects after entering into the CG5 the time and an approximate location for the centroid of the survey.

Drift corrections were further refined by measuring values at a base station established outside of Snee Hall on Cornell's campus before and after each day's operations. My field assistants and I also occasionally measured at the base station in the middle of the day when we returned to Snee for operational reasons. The CG5 readings were corrected to account for an assumed linear-with-time instrument drift by simple linear interpolation of values and time increments during the interval between base station readings.

The nominal sampling grid was designed to be on 500 meter centers. I subsequently used a GIS to deform the locations to lie on roads with public rights-of-way or Cornell owned property – mostly to avoid seeking measurement permission from a myriad of property owners. To the best of my efforts, measurements with permission from non-Cornell landowners occurred twice during the survey: once on Ithaca College land (with the assistance of Ole Gustafson), and once on the land of Six Mile Creek vinyard, with the permission of the resident manager. A base map displaying the actual locations of the measurements is shown in Figure 2.

Because of the $1/r^2$ character of the gravity field, measurement height is a sensitive parameter in reducing gravity readings. Using the Free Air rate of $3.089 \times 10^{-6} m/s^2\ /m$, a height error of about $\pm 0.016 m$ contributes to the gravity error budget the same amount as the $\pm 5 \times 10^{-8} m/s^2$ laboratory repeatability of the CG5 meter.

For this reason, modern gravity surveys often use high-precision GPS techniques for vertical positioning – such as Real Time Kinematics (RTK). In this survey, while I flagged the measurement positions for later RTK surveying, unfortunately – due to operational reasons – no RTK surveys were actually performed.

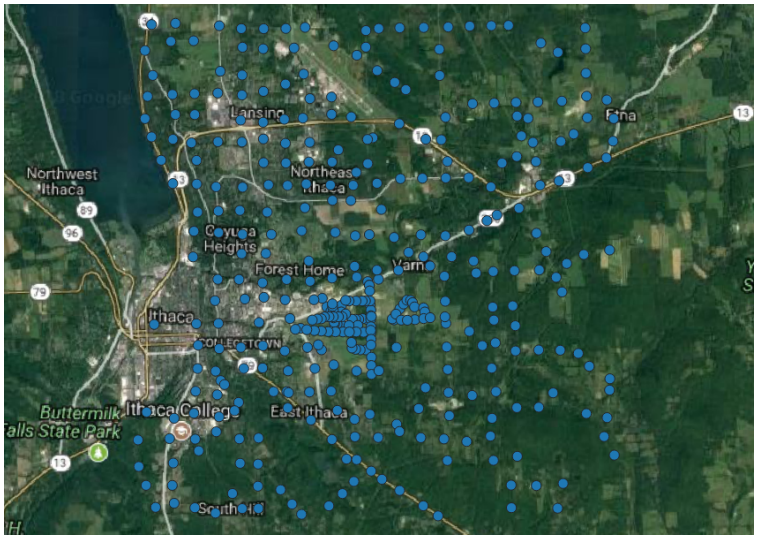

Figure 2: The locations of the 395 gravity measurement stations, plotted on a Google Maps image of the surroundings. The blue circles correspond to the brown circles in figure 1.

Instead, for vertical positioning I relied on a 2 m horizontal resolution Digital Elevation Model (DEM) available for Tompkins County[1]. That DEM is derived from a nominal 1.4m spacing, 18.5cm RMSE vertical precision, LIDAR survey commissioned by the county in 2008[2]. Horizontal positioning of the measurement sites relative to this DEM was established by a smartphone GPS rough position, refined by my locating the position on a high resolution airphoto using the Android application "Mapit GIS". This allowed horizontal location precision well within the 2 m pixel resolution of the DEM. In turn, that allowed a vertical location precision assumed to be equal to the 18.5 cm LIDAR RMSE – or about $57\mu Gal$ when converted via the Free Air rate.

For reference, the median of the 395 measured CG5 time series' standard deviations was 23 μGal. This implies that the estimated vertical positioning error contributed a little more than twice the CG5 field measurement errors to the total gravity error budget.

In addition to the tidal and drift corrections already described, I also computed the following standard corrections. 1) A latitude and normal gravity correction accounts for variations in g due to position changes on the rotating reference (GRS80) ellipsoid. 2) A free air correction accounts for changes in vertical height above the reference ellipsoid. 3) A Bouguer correction accounts for the attraction due to infinite flat slab of rock of a specified density between the reference ellipsoid and the height of a measurement. 4) A terrain correction which adjusts the Bouguer correction for the fact that there are topographic hills and valleys – not just an infinite flat slab of rock. Terrain corrections used the Oasis montaj® software package from Geosoft, along with local and regional DEMs. The final estimate after all of those corrections are applied is termed a "complete" Bouguer anomaly.

Estimation of the Bouguer correction density was performed in the spirit of Nettleton's (1939) technique, which seeks to maximally decorrelate the gravity anomaly from topography. That permits the anomaly to be solely due to underground mass distributions rather than topography. Various techniques for estimating such correction densities are summarized in Yamamoto (1999). I chose the technique of Parasnis

[1] `http://gis.ny.gov/elevation/metadata/County-2-Meter.xml`
[2] `http://gis.ny.gov/elevation/metadata/NYTompkins2008LiDARData.xml`

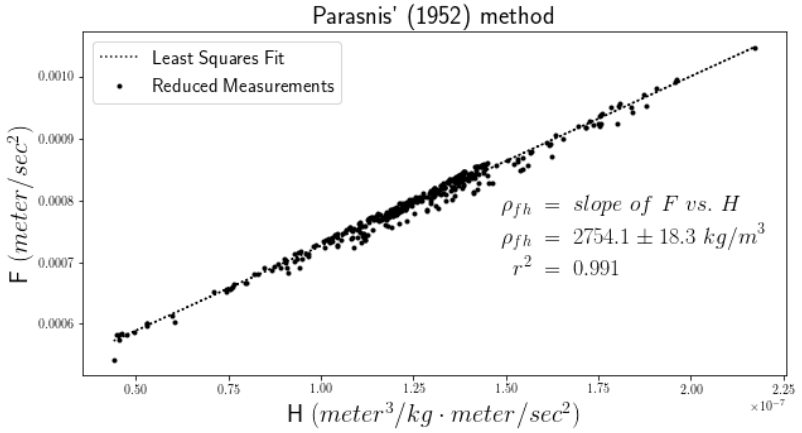

Figure 3: The Parasnis (1952) method of estimating the best Bouguer and terrain correction density. Plotted is the Free Air gravity (F) on the y axis vs. H on the x axis. The parameter H is composed of all terms in a rearrangement of the complete Bouguer anomaly formula that are proportional to the correction density (Yamamoto, 1999, eqn. 23). The slope of the resulting line is the best fitting correction density.

(1952) – termed the F vs. H technique by Yamamoto – which essentially performs a least-squares fit of Free Air gravity vs. all terms in a Bouguer correction that are proportional to density in order to estimate the best decorrelating correction density (Figure 3). Figure 4 displays the correlations for the best correcting density estimate $(2.75gm/cc)$, the "standard" estimate $(2.67gm/cc)$, and a zero correcting density estimate which corresponds to a free air anomaly. Inspection of the figure shows that a free air anomaly – advocated by researchers who primarily deal with oceanic gravity anomalies – would leave a significant correlation in the results. Since the locations of the topography around the ESH sites are already well known, little new information about the underground geological structures would be gleaned from interpreting free air anomalies from this survey. As an aside, while this Bouguer correction density analysis appears to have added little value to the results as opposed to simply using the standard correction density, in fact it enabled me to find a deeply buried error in my processing chain[3].

One curious effect was noted during the survey. The CG5 standard deviations during measurement attempts in flat sediments nearby Cayuga Lake – including downtown Ithaca – were an order of magnitude larger than those we observed in hundreds of measurements in the harder rocks of the hills. Sparked by a suggestion from Cindy Ebinger (2018, pers. comm.), and from Cladouhos et al. (1989) reporting strong isoseismals in downtown Ithaca from a regional event, I recorded a long time-series of the full 6 Hz. sampling from the meter during a quiet early morning period. I also recorded a similar long time-series during normal business hours at our base station on Cornell's campus. Power spectra of the two time series show unmistakable signs of aliasing caused by under-sampling in the downtown recording (Figure 5). I attribute that to basin amplification in the (reclaimed?) land of downtown Ithaca. Essentially the valley sediments were vibrating at high frequencies like a bowl of jelly. For that reason, plans to measure at stations in the flat sediments surrounding downtown Ithaca were abandoned. Gravity workers encountering similarly noisy gravity readings with Scintrex CG5 gravity meters in other, geologically and mechanically similar regions might want to keep such aliasing in mind.

[3] I had incorrectly used the DEM as if it were expressing heights in feet when in fact it used meters. This threw off every subsequent processing step and took significant time and effort to find.

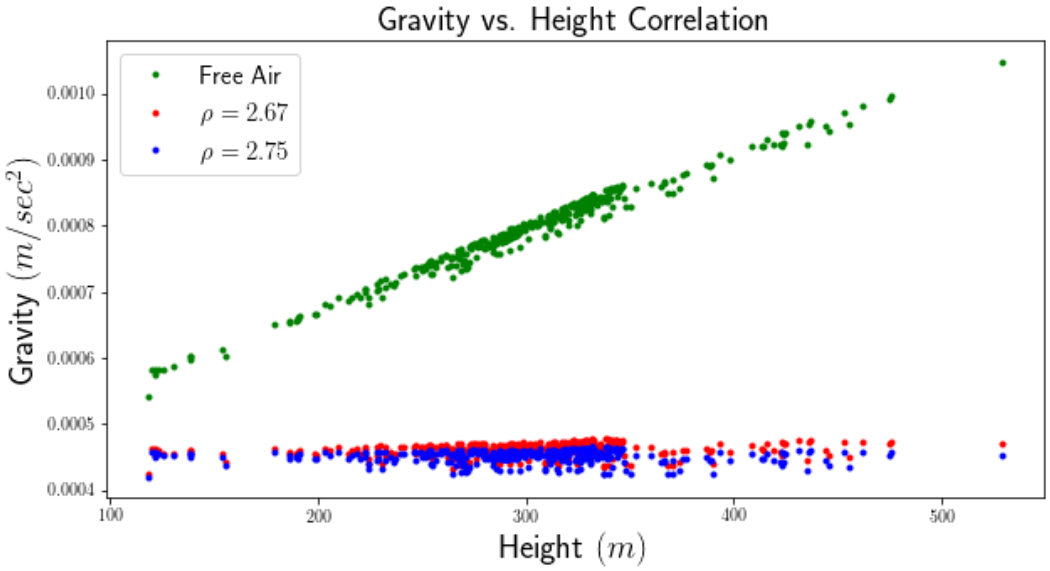

Figure 4: A correlation between gravity measurements from this survey with various corrections applied and measurement height (in meters above the reference ellipsoid). Shown in blue circles are the gravity anomaly values using the best estimate due to the technique of Parasnis (1952) for a Bouguer correction density of $(2.75gm/cc)$. Shown in red circles are the gravity anomaly values using the "standard" correction density of $(2.67gm/cc)$. Finally, shown in green circles are the free air anomaly values corresponding to a correction density of zero.

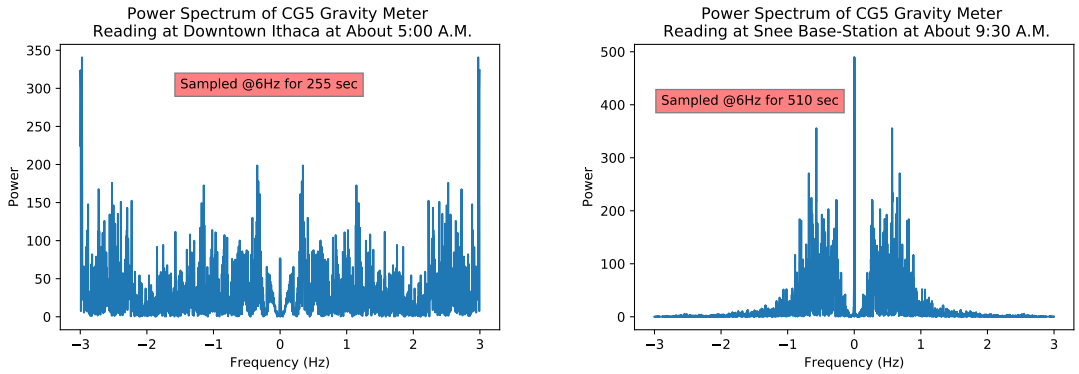

Figure 5: Power spectra of two CG5 time series of gravity measurements. Left: the spectrum obtained when measuring during a quiet time of day on the downtown Ithaca flat sediments. Right: the spectrum obtained when measuring at the Snee base station later that same day. The downtown spectrum shows clear evidence of strong power at the Nyquist frequency as well as aliasing – implying that the 6Hz sampling frequency built in to the CG5 undersampled the downtown time series. I attribute this to basin amplfication of higher frequency seismic noise in the downtown sediments. I attribute the strong DC power in the Snee spectrum to an instrument drift during the interval between two individual time series of 255 measurements concatenated to produce the 510 sample series from which the spectrum was calculated.

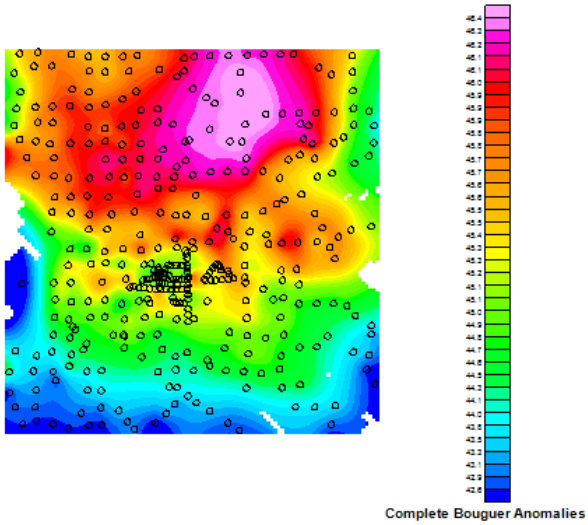

Figure 6: A minimum curvature interpolation ("gridding") of the complete Bouguer anomaly measurements. Open circles are the locations of the measurements – corresponding to the locations in previous figures. This interpolation forms the basis of the gravity analysis and interpretation discussed in subsequent sections of this report.

One final correction was performed. Because the CG5 is a relative gravity meter, it is not capable of determining the absolute value of gravity at each location. An absolute gravity station "Buffalo AA 1993" (Winester, 1993) is located at Canisius College in Buffalo, NY – about a 3 hour drive away from the field area. Buffalo AA was measured just prior to returning the CG5 to its owner. A drift correction was performed on the Buffalo AA reading in the manner described in Appendix 1, as well as the onboard tidal correction. These served to tie our base station readings with the absolute value established at the Canisius College station.

The complete Bouguer anomaly – the end result of all of the gravity measurements and corrections described above – is then interpolated onto a regularly spaced grid with 100m pixel size. I used the minimum curvature algorithm of Oasis montaj to perform the interpolation. The result, shown with the measurement locations in open circles, is displayed in Figure 6.

3 Methods 2: Aeromagnetic Measurements and Data Reductions

Much like gravity surveys, magnetic surveys also seek to identify underground distributions of geological structures. Under certain broad assumptions – applicable in the survey region – measurements of Total Magnetic Intensity (TMI) field strength yield a result that obeys the same mathematics (a Poisson equation for a scalar potential) as the result from gravity surveys (e.g. Blakely, 1996). In gravity, underground sources of the observed anomalies are due to variations in mass density. In the case of magnetic surveys, sources of anomalies are variations in the strength of magnetization. As is widely known for the kinds of rocks underneath Tompkins County, to first order, variations in the strength of magnetization correspond to variations in concentration of the mineral magnetite.

One profound difference between magnetic and gravity surveys stems from the fact that anomalies in the magnetic field being observed have a dipole character – due to magnetic induction from "illumination" by the Earth's inclined primary field. Practically speaking, this results in TMI anomalies being *offset* from their source locations – with a positive lobe on one side of the source and a corresponding negative lobe on the other side. Fortunately, there exist algorithms in the spatial Fourier domain that ameliorate that dipole character (e.g. Blakely, 1996). Two such algorithms were employed in this work. 1) Reduction To Pole (RTP) processing – which estimates the TMI field as if it were being observed at the North magnetic pole with a vertical primary ("illuminating") Earth's field. RTP preserves the dipole character of the TMI anomaly field, but essentially – for a simple point source – it moves the positive lobe and negative lobe to be concentric over the source. 2) Psuedogravity (PSG) processing – which mathematically collapses the dipole source of RTP to a monopole source at the same location. PSG is equivalent to performing a vertical integration of the RTP field – something which is possible because Laplace's equation (Poisson's equation without sources in free space) enables direct calculation of vertical derivative or integral operators in the Fourier domain. The end result is that a PSG transformed field is equivalent to a gravity field that would be observed if the magnetization strength variations were mass density variations. See Blakely (1996) for an extensive discussion of these operations.

The project purchased non-exclusive rights to aeromagnetic survey data over Tompkins County from the geophysical service company EDCON-PRJ. Flown in 1999 on speculation by that company, it was intended to support geophysical exploration for the Trenton/Black River gas play of that era. The data availability for our region was discovered by Terry Jordan in 2015 during the DOE sponsored Appalachian Basin Geothermal Play Fairway Analysis project – of which I was a research team member.

Relevant details of the survey include a nominal flight-line spacing of 1/3 mile; a nominal tie-line[4] spacing of 1 mile; a nominal ground clearance of 500 feet; and an along-line sample spacing of approximately 25 meters. The measured average ground clearance of the project's portion of the survey is 554 feet – as estimated from the onboard radar altimeter. Figure 7 shows the position of the flight and tie-lines.

Because the survey was flown over an area dense with artificial magnetic sources (such as power lines, pipelines, etc.) the project also purchased a "de-cultured" version of the gridded data. That was delivered by EDCON-PRJ along with the more conventional TMI and RTP grids. My intention in buying the de-cultured grid was to have experts perform that part of the preprocessing. Unfortunately, a side-effect of their de-culturing algorithm resulted in essentially a low-pass spatial filtering of regions far from the evident dipole artifacts. Because the worm analysis – described in the next section – relies on short spatial wavelength content for detecting shallow features, I ultimately decided to use the normal ("un-de-cultured") RTP grid for that work. The EDCON-PRJ RTP grid has 200m pixels. I also transformed that RTP grid into a PSG grid of the same resolution using Oasis montaj tools to perform the (Fourier domain) vertical integration.

An aside: the sheer measurement count – some 163,000 samples – of the raw TMI samples from the EDCON-PRJ survey would appear at first glance to support a much finer resolution grid than the 200 m spacing used here. However, recall that the average ground clearance for all the measurements was 554 feet (or about 168 m elevation) from radar altimetry. This means that the grid is already "upward continued" – i.e. removed from any possible sources – about the same distance as the grid cell size. From a spatial aliasing/sampling point of view, there might be some benefit from reducing the interpolation cell size to below the upward continuation height. However, I decided to keep the RTP grid exactly as delivered from EDCON-PRJ and use that as the basis for further processing. Any future work based on these magnetic data might consider reducing the interpolation resolution to something like a 100 m cell size to preserve spatial

[4] Tie lines are used to correct – or "level" – for instrumental and magnetic field temporal drifts between flight lines.

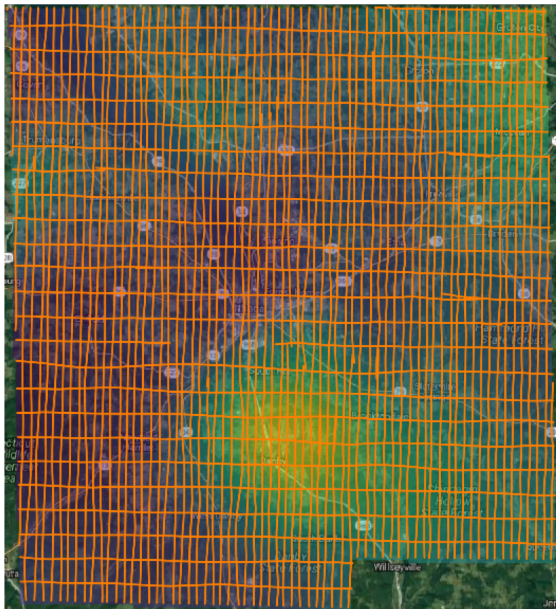

Figure 7: Flight and tie-line locations purchased for Tompkins County from the EDCON-PRJ aeromagnetic survey. The faint colors are intensities of the RTP transformed field. The background is a Google Maps air photo of the region.

oversampling after upward continuation.

Figure 8 shows a map of the TMI grid from EDCON-PRJ. Figure 9 shows the corresponding RTP grid. In both cases, EDCON-PRJ has used the graphical technique of hill-shading to visually enhance short wavelength features in roughly WNW-ESE orientations.

4 Background: Poisson Wavelet Multiscale Edge Detection (Worms)

There is a vast literature on methods of processing PF data for interpretation. Blakely (1996) presents a nice overview of the main classes of techniques. Many – if not most – of the techniques suffer from the well known inherent non-uniqueness of potential fields – where infinite families of different underground source distributions generate exactly the same measured field. In particular, inversions for source distribution models commonly constrain vastly more degrees-of-freedom via the regularization assumption (such as "smoothness" or minimum energy in edges) than they constrain from the measured data.

I do not trust poorly regularized inversions. In my opinion they impose un-geological or even un-physical constraints on the behavior of the rocks simply to arrange for a "solution" to the ill-posed mathematical inverse problem. I accept that my opinion is not popular among many other practitioners of PF analysis.

In contrast a simple, testable, regularization of "Rocks Have Edges" lies at the heart of detecting geological structures using the Poisson wavelet multi-scale edge analysis of potential fields – informally known for brevity as the 'worm' technique – my co-workers and I developed starting nearly 20 years ago: Hornby et al. (1999)[5] (independently derived by Moreau et al., 1997). This technique, widely deployed in

[5] Google Scholar lists 227 citations of this paper as of this writing.

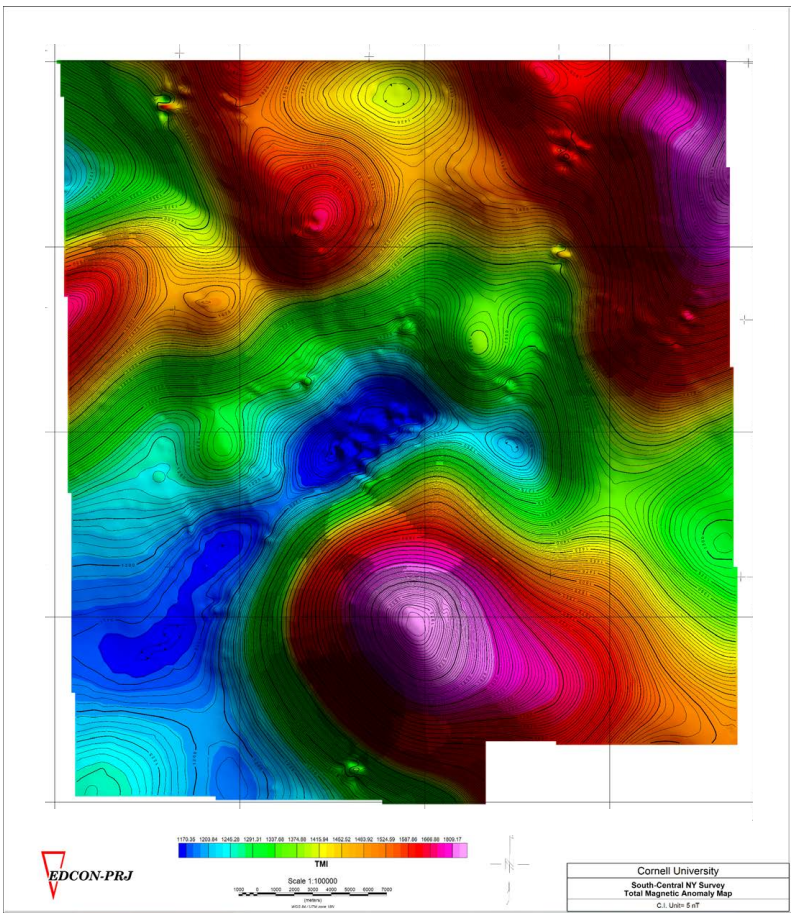

Figure 8: Total Magnetic Intensity (TMI) map from the EDCON-PRJ aeromagnetic survey.

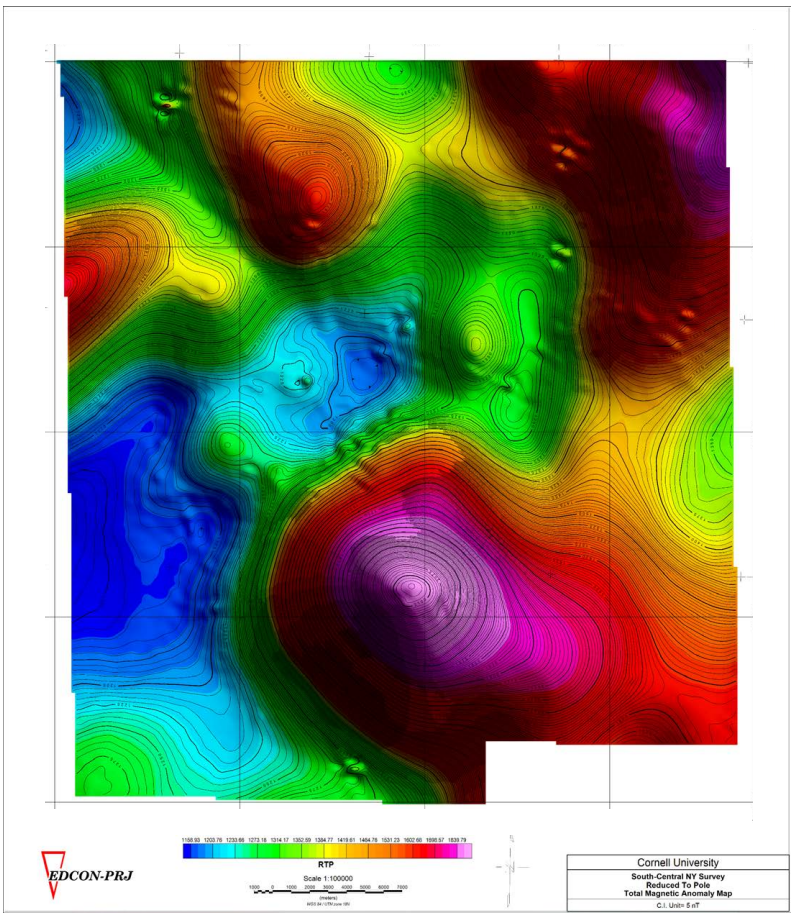

Figure 9: Reduced To Pole (RTP) map from the EDCON-PRJ aeromagnetic survey.

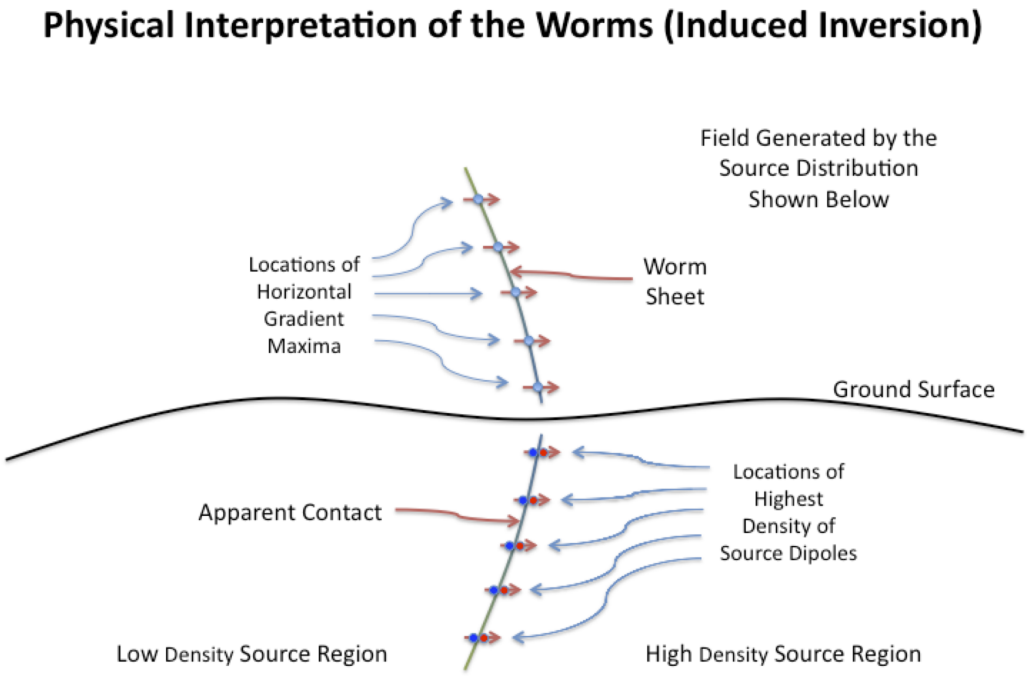

Figure 10: A vertical cross-section cartoon of the worm technique. The gravity or magnetic field is nominally known completely at the ground surface. The field is upward continued to a suite of heights. Hornby et al. (1999) show that each level of upward continuation corresponds to a (continuous) wavelet scale. The locations of maxima in the horizontal gradient of the field at each height become an edge (or a 'worm') for the corresponding scale (the intersection of these 1D features with the plane of section are shown as blue dots above ground), the collection of edges at all scales are 'multiscale edges'. A suite of worms arising from connected locations on the ground is a 'worm sheet'. As explained in the text, an underground inversion is induced via a physical interpretation of the inverse wavelet transform as a distribution of dipole sources. Draping the worm sheets underground (blue and red dots) results in a visualization of the locations of highest density of dipole sources. These are interpreted as the locations of apparent lateral contacts.

the mining community in Australia and elsewhere (e.g. GoldCorp, 2001), uses gravity and magnetic fields to detect lateral contrasts ("edges") in mass density or magnetization strength respectively. Figure 10 displays a cartoon summary of the technique.

Some theoretical advantages of the technique include:

- Marrying wavelet theory and potential field physics by building a wavelet from the Green's function of the Poisson equation (Laplace's equation with sources).
- The inverse wavelet transform has a physical interpretation as an *induced* inversion to a dipole source distribution (Boschetti et al., 2001; Hornby et al., 2002) that produces a field that is exactly the starting field. Stated once again, the regularizing assumption is that 'Rocks Have Edges'.
- The field values at the locations of the multiscale edges (worms) alone, when combined with the inverse wavelet transform above, can produce a field that is a close approximation of the starting field via the result from Mallat and Zhong (1992).

Hornby et al. (1999) show that the magnitude of the horizontal gradient – normalized appropriately to correspond with wavelet theory – changes amplitude with upward continuation/scale-change in such a fashion as to identify the Lipschitz exponent (related to the fractal dimension) of the underlying singularity in the source distribution. That is, if we define

$$M \equiv (z/z_0)||\overrightarrow{\partial f/\partial x} + \overrightarrow{\partial f/\partial y}|| \tag{1}$$

where f is our potential field (e.g. $f = ||g_z||$ for gravity surveys, or $f = \mathrm{pseudogravity}$ for magnetic surveys) then $\partial M/\partial z$ is the quantity of interest in determining the Lipschitz exponent. In this way, underground singular sources are classified as having 0, 1, 2, 3 dimensions, or even something fractal with dimensionality in between the integers. Fortunately, the lateral discontinuities between 3D sources are the edges that most strongly persist with upward continuation – enabling the simplified interpretation shown in Figure 10. M is usually displayed as the worm color, and one can visually assess $\partial M/\partial z$ from the graphical representation.

The Lipschitz exponent concept is closely related to the geophysically-more-widely-known 'structural index' from Euler deconvolution (e.g. Reid et al., 1990). A masters thesis (Navarrete, 2015) has shown that the locations of worms and Euler solution routinely coincide, but that the worm technique offers significantly enhanced lateral coverage over the Euler deconvolution solutions.

Some practical advantages of the worm method include:

- When draped underground as in Figure 10, the worms resemble lateral contacts and reproduce (at least near the surface) the sense of dip of the contact. This provides an immediate cue towards a sensible geologic interpretation. Unfortunately – once getting beyond 'shallow' and 'steep' – the magnitude of dip is more problematic, since the field is due to more than one body and interactions between sources cause complexities. Jessell (2001) summarizes a large number of cases of worm behavior for different structural geologic settings.

- The worms commonly extend information about lateral discontinuities over large regions. This offers the geological interpreter a chance to connect structures that might not be recognized as being related.

- Deep worms tend to represent (smoothed) major lateral boundaries. By following the worm sheets upwards, the connected shallow expressions can be identified. At the scale of our surveys those major lateral boundaries are likely to be the major geological structures in the area.

The worms are best visualized in 3 dimensions in order to see their interrelations. In previous efforts, that has led to working with them primarily in graphical visualization packages such as VTK (Schroeder et al., 2004) and VisIt (Childs et al., 2005) or commercial mining industry visualization packages such as FracSIS (RungePincockMinarco, 2015). For this project, we need to incorporate the worms with other GIS information, but few GIS packages deal fluidly with 3D visualization. ArcScene – a component of ArcGIS – can in fact display 3D GIS information, but worms present a serious performance problem for ArcScene due to the large number of individual items that must be displayed. For this project, I work around this problem by displaying worms from a restricted series of depths in 2D map view in QGis, but the results are less useful than a wished-for performant 3D GIS could produce.

5 Results: Gravity and Magnetic Worms

The gravity grid of Figure 6 was used for gravity worming. Both a PSG and an RTP grid from the grid data underlying Figure 9 were used for magnetic worming. Because the PSG data were so smooth, I actually

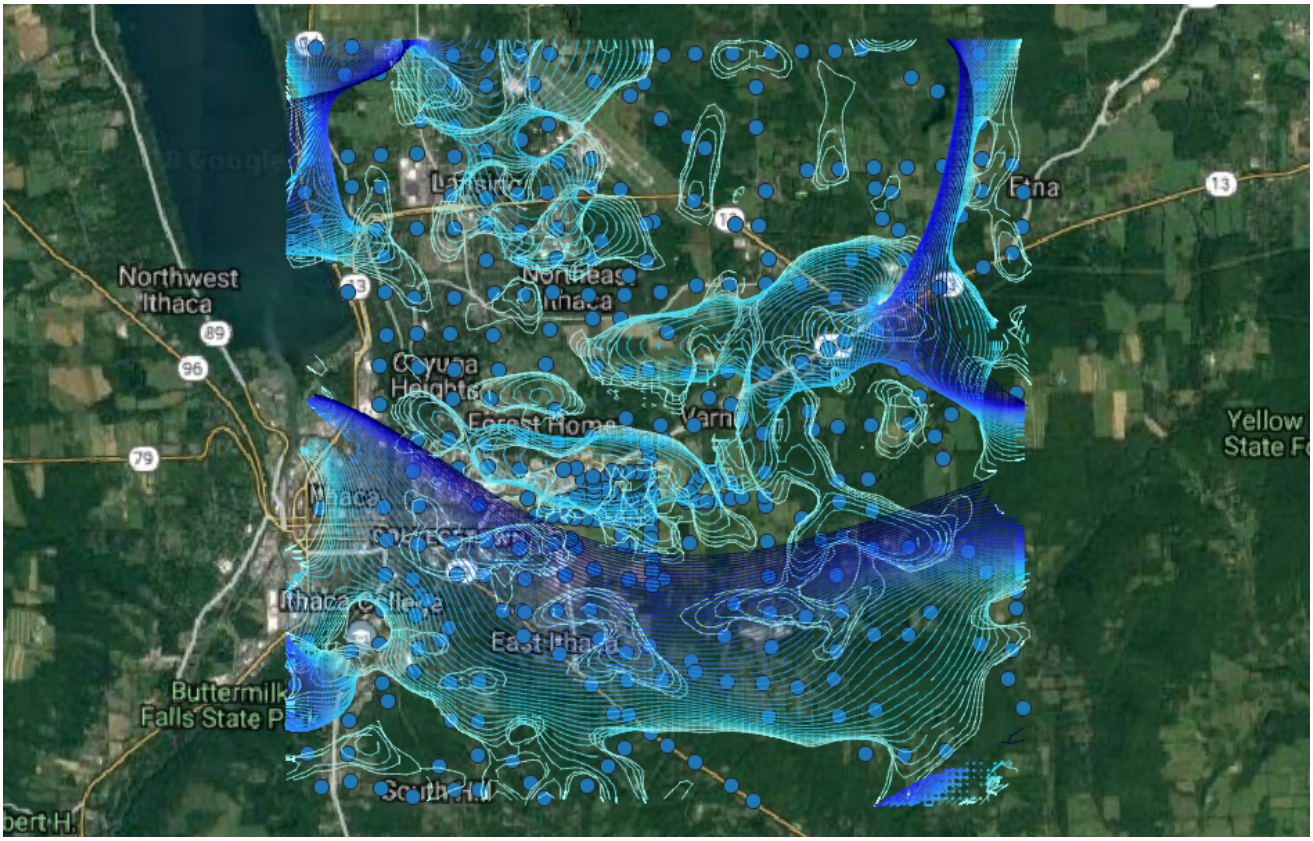

Figure 11: Gravity worms over the entire survey area. The worms are in 100 meter depth contours, with the shallowest level of 100 m in light blue, grading to the deepest level of 5000 m in dark blue/black. Gravity station measurement locations are indicated by the blue circles, with a Google Maps base map.

interpreted the RTP worms. Recall that the RTP corresponds to the 1st vertical derivative of the PSG, and that 1st vertical derivatives are a well known detail enhancing operation in PF processing.

I used the BSDWormer software described by Horowitz and Gaede (2014) to compute the gravity and magnetic worms from the Bouguer and RTP grids respectively. These grids had been pre-processed by the MAGMAP module of Oasis montaj for the spatial Fourier domain upward continuation operations performed by BSDWormer. That pre-processing included de-meaning the grids. It also included a spatial boundary padding (similar in spirit to Hann or Hamming tapering/"apodization") of the grids in order to remove troublesome short wavelength Fourier components due solely to the sharp boundary steps at the edges of the surveys.

Shown in Figure 11 are the gravity worms for the whole gravity survey region. Shown in Figure 12 are the (RTP) magnetic worms for the whole of the Tompkins County survey area.

Zooming in to the region of the proposed drilling sites, a map view of the gravity worms is shown in Figure 13. The 3 dimensional character of the worms is difficult to discern from the map view, but examination in the 3D visualization environment Paraview yields more interpretable results (Figure 14). For completeness, a view of the RTP magnetic worms over the same map coverage is shown in Figure 15.

At this level of detail, it is often worthwhile to ignore the shallowest level or two of worms, since their structure can be dominated by measurement noise or spatial aliasing due to very short characteristic

Figure 12: Magnetic worms over the entire survey area. The worms are in 100 meter depth contours, with the shallowest level of 100 m in light green, grading to the deepest level of 5000 m in dark green/black. A Google Maps image of the area serves as a base map.

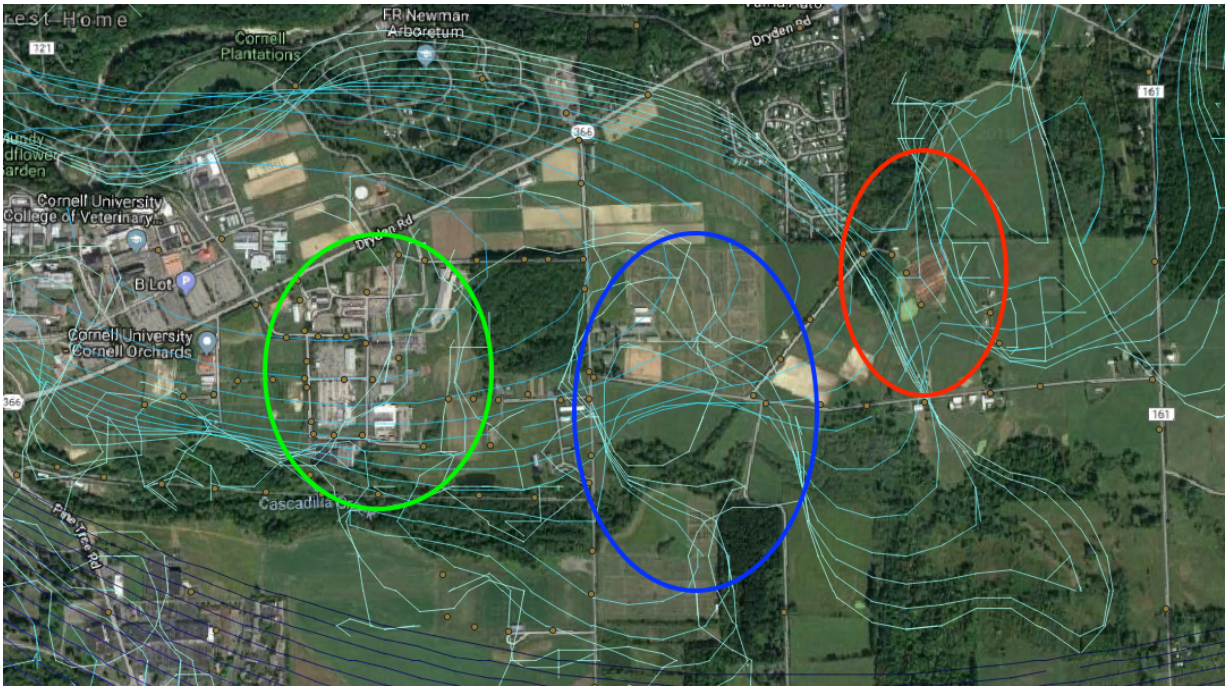

Figure 13: A map view of the gravity worms of Figure 11 zoomed in to a region nearby to the proposed drilling sites. The light brown circles are the gravity measurement stations, as before. The colored ovals correspond to structures that will also be shown in the 3D perspective view of Figure 14.

length source variations. This is particularly true of gravity worms, since they are measured at ground level. It is somewhat less of an effect for aeromagnetic surveys, since sampling the field above the ground surface automatically decreases short wavelengths (by upward continuation).

6 Interpretation

It is worth stating at the outset that this work is in the fortunate position of having seismic reflection surveys in the vicinity – both those performed recently by Larry Brown, and the older oil-and-gas surveys purchased from commercial vendors. My interpretations are thus able to be confirmed (or refuted) by a well-trusted, high-resolution – even if geographically limited – technique! I greatly look forward to being able to participate in future work that integrates all of the information gleaned from the PF, the seismic, the borehole log interpretation, and other techniques being performed for the ESH project.

There are several geological structures found by this work. Some of them are previously known or have been inferred, while several of them are new.

6.1 A Large, Deep Structure South of the Proposed Drilling Sites

The primary large structure relevant to ESH – possibly identified in both the gravity and the magnetic analyses – is the major deep structure south of the proposed drilling sites. In the magnetic worm analysis, it appears as the large, deep, roughly comma-shaped feature in the south and east of Figure 12. It also corresponds to the large magnetic high in the south of both Figure 8 and Figure 9. In the vicinity of the

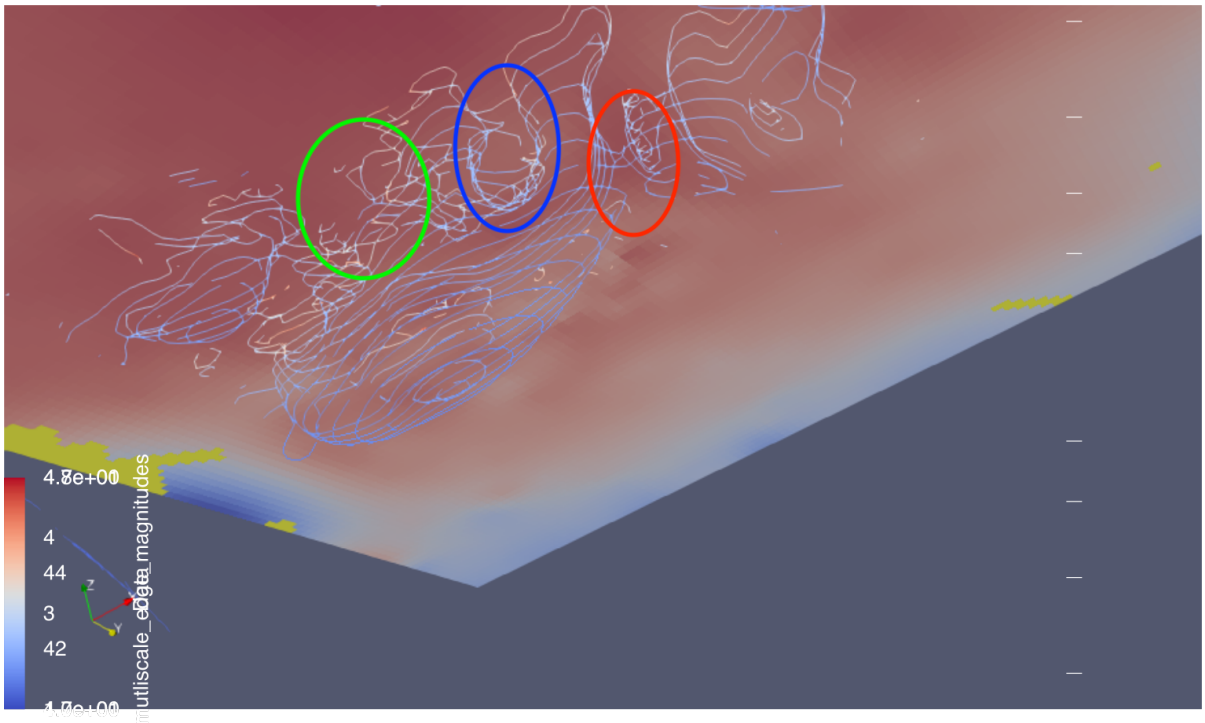

Figure 14: A perspective view of the gravity worms of Figure 13. The view is underground, from the SE looking upwards to the NW. The image at the surface is the Bouguer gravity field of Figure 6 with the same geographical extent. Colored ovals correspond to the same structures (with the same color scheme) as the ovals in Figure 13. The image contains roughly the same map-view subset of worms as in that figure, but limited in depth to less than about 2000 m. Rather than being colored by depth, the worms are colored by the quantity M as defined by equation 1.

Figure 15: A zoomed map view of the RTP magnetic worms over the same coverage region as that of Figure 13. There are only a few worms evident in the W and SW parts of the region.

proposed drilling sites, the magnetic worms suggest that the "lateral discontinuity" dips to the south – by virtue of the deeper worms appearing to the south of the shallower worms in that region of Figure 12.

In the gravity worm analysis, a nearby major deep structure is also evident in the south of Figure 11. The spatial correspondence is perhaps best viewed in the overview image of Figure 1. While, due to the spatial proximity of the strong gravity and the magnetic features, it is tempting to interpret these as representing the same feature, the evidence is not conclusive. In particular, as is evident via the deeper gravity worms to the north of the shallower worms in Figure 11, the structure inferred from gravity appears to dip to the north. This contradicts the interpreted sense of dip from the magnetic worm analysis. A possible explanation is that there are *two* co-located features in the region, but I judge that to be too much of a coincidence to be confident with that interpretation. I will leave it to confirmation from the seismic reflection work to decipher this apparent difference.

In Podwysocki et al. (1982, Appendix E), Jeff Phillips and others from the USGS interpret such large – roughly circular – positive magnetic anomalies in this region as (intrusive) mafic plutons in the rocks of the basement. I see no evidence from this work to contradict that, and so I proceed accepting their interpretation at face value.

The implications of a nearby pluton (at depth) for geothermal heat in our region are (at least) twofold. From the perspective of the ESH project, the news might be good or it might be bad.

Firstly, the pluton itself potentially contains a higher concentration of radioactive elements (K, U, Th) than the surrounding country rocks of the basement. Carrying on with Phillips' interpretation of the pluton being precambrian in age, it is confined to being beneath the basal erosional contact of the Appalachian Basin sediments. That means depths greater than about 3km for the situation underneath Ithaca. Those radioactive elements are an important source of geothermal heat. Somewhat counterbalancing that, the

precambrian age of the inferred pluton means that much of that radioactive heat source has had hundreds of millions of years to decay since emplacement. In other words, it might only be a weak (additional) source of heat augmenting the basal heat flux from lower in the crust.

Secondly, by virtue of being intruded into different basement rock types – with assumed different thermal conductivities – the pluton *may* locally "refract" heat flux lines (more properly for 3D, flux sheets) from deeper sources. Whether the pluton *concentrates* those lines into its interior or *repels* those lines into its exterior depends on the relative values of thermal conductivities of the pluton vs. the surrounding rocks. In either case, the local conductive heat gradients affecting the proposed ESH drilling sites would be affected – both in the sediments, and in the underlying basement rocks. The news for the ESH project could be good since repelling flux lines locally should enhance conductive heat flow in the sediments at the ESH site. The news for the sediments could also be bad if the mafic plutonic rocks concentrate the heat flux into the interior of the intrusion. Further confounding these suggested effects, the pluton's burial depth means that the heat fluxes in the overlying sediments would no longer remain as concentrated as in the basement.

Barring definitive evidence, I suggest that some (2D or 3D) heat flow modeling of the situation might be appropriate to clarify the different effects. Perhaps as an M.Eng. project for some student?

6.2 Structures in the Immediate Vicinity of the Proposed Drilling Sites

Turning now to nearby the proposed drilling sites, concentrate first on the gravity analysis worms in the green oval of Figure 13 and Figure 14. From the 3D environment of paraview – unfortunately not readily apparent in the static images of this report – it is clear that there are 2-300 meters in depth of incoherent "noisy" gravity worms. For the reasons mentioned above, I think these features are not worth paying much attention to. More coherently, below this "surface clutter", there are a closed set of worms that appear to be an elongated "bowl" shape. The closure of that bowl is commonly observed and not very significant – it just means that there is a stronger feature off to the side that dominates the local horizontal gradients in the field. The feature on the south side of that "bowl" – dipping to the north underneath Cascadilla Creek – is more significant. I'm interpreting that as a geological boundary of some sort in the rocks – perhaps a minor fault or maybe even a paleo-gorge later filled more recent glacial sediments given the glacial history of the Ithaca region. The corresponding north edge of the "bowl" feature appears to be connected to the south edge via the east and west closures of the worms. This is more consistent with the gorge interpretation than with the fault interpretation. However, it could also be a minor graben which is consistent with the minor fault interpretation. Supporting either interpretation is the fact that the longer characteristic length feature underlying the worms is a gravity low – suggesting less dense rocks lie below the feature. The depth extent of the structure is likely limited by the deepest worm evident – 1400 m in depth. That should be well above any operating depths of the proposed ESH activities. Note also that the magnetic worm structures appearing in the west of Figure 15 align with the axis of the "bowl" structure evident in the gravity worms – suggesting confirmation of this structure by both techniques. If my interpretations as to depth (depth being one of the harder things to interpret with confidence using the worm technique) is confirmed by the seismic reflection work, I do not expect this structure to be troublesome for the ESH project.

Next, turn to the blue oval of Figure 13 and Figure 14 where the "surface clutter" is less pronounced. Once again the 3D environment of paraview provides an informative view. The sub-vertical structures striking NNW-SSE are likely to be significant. The overall connectivity and form of the set of worms between the blue and red ovals lend support to the paleo-gorge interpretation of the green oval structures. However, the fact that the worms in the blue oval would form an "overhanging topographic promontory" under that interpretation is quite troublesome. I'll focus on the sub-vertical structures inside the blue oval

and interpret them as shallow contacts. Were those contacts to occur at depths relevant for ESH operations, they might be of concern. However, they are fairly clearly at shallower depths – appearing to range down to about 5-600m before being overshadowed by larger scale anomalies. Once again, should the seismic reflection work confirm this interpretation, I also do not expect these structures to be troublesome for the ESH project.

For the NNW-SSE structures appearing in the red oval of Figure 13 and Figure 14, many of the same comments apply as for the blue oval above. A difference is that the structures appears to terminate even more shallowly than those in the blue oval. Once again, I do not expect these structures to be a problem for the ESH project.

6.3 Structure in the Vicinity of the Salt Mine up Cayuga Lake

There are many other structures apparent in both the gravity and in the magnetic surveys of Figures 11 and 12. Most of them are not interpreted in this report since – in my opinion – they are not of immediate relevance to the ESH project. However, I draw your attention to the more-or-less E-W structure intersecting Cayuga Lake by the salt mine just south of Myers Point in Figure 12. This *apparently deep* structure is nearby to an outcropping shallow fault that has been mapped by numerous Cornell Geology students during field exercises. It is also nearby both to a reverse fault and to the axis of the Fig Tree Anticline mapped in the Stone & Webster Engineering Corporation et al. (1978) generalized geology map that forms the background of Figure 1.

In my opinion this feature is relevant to the ESH project because Prof. Keranen reported on micro-seismic activity located in the vicinity of the feature. I was initially skeptical of attributing that micro-seismic activity to current tectonic stresses on a fault due to its proximity to the underground workings of the salt mine. In mining, rockfalls – and even rockbursts – occur much more frequently than in the surrounding rocks due to the perturbation of the regional stress field by the voids, sharp corners, etc. of the underground workings. *The worm structure mentioned above caused me to change my mind.* I now interpret this structure as evidence supporting Prof. Keranen's interpretation of the recorded micro-seismicity as being due to activity on a fault – rather than being solely due to a side effect of mine workings. There have been discussions about deploying a passive seismic array in the region surrounding this area. I would strongly support such a deployment, since it would enable much better locations for the micro-seismicity – particularly improving estimates of depths to the events. Should the depths be well constrained to lie below the mine workings, that would be strong evidence supporting the existence of fault activity. Should the locations also lie nearby this worm feature, as well as any fault plane solutions obtained being sub-vertical with the same strike, I would regard the worm feature as being the location of a fault.

Should all of the inferences in the above paragraph be borne out, it is worth noting that the feature being discussed approximately shares its apparent strike with the boundary of the inferred pluton just to the south of the proposed drilling sites – discussed in section 6.1 above. This correlation between strikes may be significant for ESH operation. That significance derives from an interpretation of the orientation of a fault in a regional stress field being relevant to Mohr-Coulomb failure along that fault. Without being drawn into a philosophical debate about the relevance of Mohr-Coulomb failure to the physics of seismicity, such interpretations must be considered by the ESH project. This is because structures of that orientation are nearly "critically stressed" and injecting into a fault of that orientation would lead to easy failure under that interpretation of seismicity.

7 Principal Recommendations

- Compare the structures identified by this work with those identified in the seismic reflection work.
- Avoid injecting into the inferred pluton boundary structure discussed in section 6.1.
- Integrate the information of this work, the seismic reflection work, the well-logging work, and any other information gleaned about the status of the underground into a uniform interpretation.
- Model the conductive heat flux situation around the inferred pluton with an eye towards understanding the pluton's effects on the proposed ESH project.
- Deploy a passive seismic array surrounding the feature described in section 6.3 with an eye towards confirming the interpretation of it being an active fault.
  - If confirmed, structures of that orientation appear to be near critical stressing. Avoid injecting near any structures found in that orientation – whether identified by this technique, seismic, or any other technique of exploration geophysics.

Appendices

Station Name	Line_Number	Date and Time	CG5 Reading	CG5 SD
Snee Base	0_1	2018-07-30 09:49:35-04	4916.335	0.011
Buffalo AA	0_100	2018-07-30 14:49:51-04	4977.229	0.010
Buffalo AA	0_101	2018-07-30 14:51:18-04	4977.230	0.010
Snee Base	0_1	2018-07-30 19:11:11-04	4916.344	0.009
Snee Base	0_2	2018-07-30 19:12:35-04	4916.344	0.011
Snee Base	0_3	2018-07-30 19:14:02-04	4916.346	0.012
Snee Base	0_4	2018-07-30 19:19:10-04	4916.354	0.014
Snee Base	0_5	2018-07-30 19:22:43-04	4916.352	0.010

Table A1: Measurements performed to tie the relative CG5 gravity survey with the absolute gravity value recorded at Buffalo AA. Times are in postgres "timestamp with timezone" format, denoting the offset from UTC as "-04" hours. Readings and standard deviations – denoted SD – are in milliGals. Line_Number pairs are not unique in the database.

1 Gravity Survey Tie to Absolute Gravity Station Buffalo AA

Winester (1993) describes the closest recoverable[6] absolute gravity station found for this work – Buffalo AA. He reports an absolute gravity value of 980351.332 ± 0.005 mGals.

On 30 July 2018, I completed a measurement loop in order to tie our survey with Buffalo AA. The loop consisted of a CG5 reading at Snee Base in the morning; 2 readings at Buffalo AA – with the kind assistance of Mark Castner of Canisius College – letting the meter settle approximately 2 hours after the 3 hour car journey; and 5 readings of Snee Base immediately after returning to Cornell's campus. Table A1 details the measurements. The location of Snee Base is 377922.91 East, and 4700093.38 North in UTM18N coordinates – near the northern edge of the paved approach path to the Snee Hall first floor entrance on the east side of the building. The location of Buffalo AA is described in Winester (1993).

Tying absolute and relative gravity station measurements is commonly done in two steps (Holom and Oldow, 2007). First, one corrects the relative meter readings for meter drift and tide at the absolute station and at the relative-survey base station. Next, one calculates the difference between corrected relative readings at the two stations. This difference is added as an increment to the absolute reading and assigned as the g value at the relative base station.

As before, I assume a linear form for the drift because I have no additional information about the functional form of the drift curve. From the values in table A1, the difference between the time of the morning Snee Base reading and the mean start time of the Buffalo AA readings is 5.016528 hours. Similarly, the difference between the time of the morning Snee Base reading and the mean start time of the evening Snee Base readings is 9.439222 hours. Since those time values are ultimately derived from GPS timings, I assume their differences are error free.

The mean of the CG5 readings at Buffalo AA is 4977.229 ± 0.007 milliGals. The mean of the evening Snee Base gravity readings is 4916.348 ± 0.005 milliGals. Both errors have been propagated as if the readings were independent. Here – as in the rest of this appendix – I use the linear error propagation

[6] A closer documented station might be found in the Syracuse airport terminal: `http://www.gis.utep.edu/subpages/states/documents/NewYork/syacuse%20j.pdf`. However, the documentation mentions that the site was due for remodeling in 1995. While I only discovered this station after the fact, given the risk that the remodeling might have destroyed the monument, and the current state of airport terminal security precautions, perhaps recovering the station might be more trouble than it is worth in the future? At the very least some reconnaissance without a gravity meter might be prudent.

software package "uncertainties" for calculations (Lebigot, 2018). The Snee Base evening reading minus the Snee Base starting reading (i.e. the total meter drift for the day) is 0.013 ± 0.012 milliGals. The fraction of that drift occurring in the time interval from the Snee Base morning reading to the Buffalo AA mean reading is $5.016528/9.439222 = 0.53145$. Hence, the total meter drift from the Snee Base morning reading to the Buffalo AA mean reading is 0.007 ± 0.006 milliGals. Subtracting that meter drift estimate from the Buffalo AA meter reading we find the drift corrected CG5 reading for Buffalo AA is 4977.223 ± 0.010 milliGals. The difference between the morning Snee Base reading – with an assigned drift of zero – and that drift corrected Buffalo AA CG5 reading is:

$$\Delta g = -60.888 \pm 0.009 \text{ milliGals.}$$

Tide corrections, as before, are computed on-board the meter. This correction is only approximate for the case of the reading at Buffalo AA, since the meter's tide calculation was set to be appropriate for the vicinity of the Ithaca survey. However, I will accept this approximation for the purposes of this report – which after all only uses gradients of a field for which all of this computation yields a constant offset. The actual tide corrections are recorded in the raw meter database, and a more refined correction could be applied in the future if desired.

The end result of this computation is that summing Δg from above with the absolute gravity measurement from Buffalo AA yields our "tied" estimate of the acceleration due to gravity at Snee Base:

$$\boxed{g_{\text{tied}} = 980290.444 \pm 0.010 \text{ milliGals.}}$$

2 Accompanying Data Files

An accompanying DVD holds the set of data files listed in Table B2. Please ask the PI (Jeff Tester) for copies of the files, since I am unsure of the distribution policy for the ESH project. A brief explanation of my choice of file formats is in order.

Most of my working vector GIS files are contained in a Postgresql/PostGIS database system on my computer. Such database tables could, in principle, be exported as ARCInfo shapefiles – which are notoriously unmanageable for novice GIS users. Instead, I migrated those database structures to self-contained spatialite[7] files. These are single file databases – including an on-board database engine – that maintain all of the "many-to-many" relations between tables in the original database tables. (Consult your local database guru if that sentence is gibberish to you.) Many GIS software packages can directly read/write spatialite database files – including ArcGIS, the open-source QGIS system, as well as the command-line GDAL/OGR system. In particular, plotting the "levels_points" table contained within the spatialite files with your favorite GIS system will show the worms in a GIS. For reference, spatialite is the spatially-enabled extension of the Sqlite database system. Sqlite is currently extremely well known and widely supported, since it has literally billions of installations – being embedded in smartphones. Given this, I expect that the spatialite file format will persist and be readable a very long time.

For raster GIS files, there are a plethora of formats to choose from. Many – such as geotiff format – are a reasonable format for interchange. However, I chose the ERMapper .ers format specifically for the following reason. The raster file itself – without the .ers extension – is in a simple IEEE binary floating point format containing the image data in raster-line order (top to bottom). The files with .ers extensions describe – in plain text – the layout, pixel size, location, and coordinate reference systems of the raster.

[7] `https://www.gaia-gis.it/fossil/libspatialite/index`

Name	Description
ESHGrav.sqlite	Self-contained spatialite database containing Complete Bouguer Anomaly worm data.
ESGBouguer.schema	Spatialite SQL commands to translate gravity database from PostGIS to spatialite.
ESHMag.sqlite	Self-contained spatialite database containing RTP Anomaly worm data.
ESHMag_rtp.schema	Spatialite SQL commands to translate magnetic database from PostGIS to spatialite.
CornellESHBouguerComplete*	ERMapper formatted grid of complete Bouguer anomaly. The unadorned file is the Floating Point format grid in raster-line order. The .ers file is the header information identifying the grid layout, coordinate system (UTM18N) etc. The .ers.aux.xml file contains some descriptive statistics of the values contained in the raster. This format can be read by ArcGIS, QGIS, GDAL, etc.
CornellESHBouguerComplete_padded*	Same as above, but padded with a smoothed taper intended to reduce spatial Fourier domain artifacts from short wavelengths introduced by step changes in value at the boundary of the interpolation.
CornellESHMag_rtp*	ERMapper formatted grid of the magnetic RTP anomaly. Filename endings have the same interpretation as described above.
CornellESHMag_rtp_padded*	Same as above, but padded in the same fashion as the gravity grid.
ESHGravityWormsAndMap.pdf	A pdf containing a live 3D model of the gravity worms, placed underneath a transparent map of the region.(1)
ESHMagneticWormsAndMap.pdf	A pdf containing a live 3D model of the magnetic worms, placed underneath a transparent map of the region.(1)
ESHGravAndMagneticWormsAndMap.pdf	A pdf containing a live 3D model of both the gravity and the magnetic worms, placed underneath a transparent map of the region.(1)
CompleteBouguerForReport.csv	Comma separated values of the gravity data and corrections. Every station other than "SneeBase" has correction values applied relative to Snee Base in columns with titles containing "RTSB". The values in the SneeBase row are different. The "meter reading" is the value tied to the Buffalo AA absolute station as descibed in Appendix 1. Additionally, the terrain correction applied to Snee Base only uses the "Regional" correction value, since the license lapsed for the software used to apply the local correction.
RegionalTerrainCorrectionGridUTM18n*	Regional Terrain Correction 2m resolution grid estimated by Oasis Montaj for a density of 2.67 gm/cc. Terrain correction is a linear operator, so this can be rescaled to whatever correction density is desired by scalar multiplication. This grid was estimated using the regional DEM described below.
OriginalMagFilesFromEdconPRJ	A folder containing the complete set of original data files Cornell PurchasedLicensed from Edcon PRJ for this project. N.B. The license agreement Cornell has with Edcon PRJ imposes certain restrictions on Cornell's ability to distribute these data. Please consult the agreement for further details.
FrankHorowitzDataLicense9032D.doc	A Word file containing the text of the license Cornell holds from Edcon PRJ to use/distribute the raw magnetic data in the above folder.

Table B2: Data files accompanying this report.

GDAL, QGIS, and most likely ArcGIS (untested) can deal with such files easily. However, the simplicity of the binary format along with the descriptive headers in the .ers files are fairly bullet and future proof. (I daresay a 1970s FORTRAN IV programmer could read such files trivially – as could a BASIC programmer.) I expect that such files could be successfully read well beyond my lifetime. Conversion to other formats is straightforward with GDAL or other GIS tools.

Most of the pdfs have a note (1) in the Description column. Those pdfs contain live 3D displays of the worms that can be rotated and zoomed interactively. Open any of those files in any recent version of Adobe Acrobat Reader – other pdf handling software is not known to work. Once open, enable the 3D content via the popup. (I need to allow "one-time only", instead of "always", in order to get it to work for some unexplained reason.) Place the cursor over the main field, and click it. In my version of Acrobat, the image only appears after that click. Now left-click-and-drag the mouse around to rotate the 3D data. My mouse wheel zooms the view; you might have to experiment. There is a toolbar above the main view that allows you to do things like reset the viewpoint, pan (instead of rotate) with the mouse, and other operations. There is also a vertical exaggeration widget at the bottom – the data are best interpreted at 1X vertical exaggeration. Please ignore the "Regional Bouguer Anomaly" title. I couldn't convince my 3D PDF generating software to stop printing that.

References

Blakely, R. J. (1996). *Potential Theory in Gravity and Magnetic Applications*. Cambridge University Press, Cambridge. Available from: http://dx.doi.org/10.1017/CBO9780511549816.

Boschetti, F., Hornby, P., and Horowitz, F. G. (2001). Wavelet Based Inversion of Gravity Data. *Exploration Geophysics*, 32,(1):48–55. Available from: http://dx.doi.org/10.1071/EG01048.

Childs, H., Brugger, E. S., Bonnell, K. S., Meredith, J. S., Miller, M., Whitlock, B. J., and Max, N. (2005). A Contract-Based system for large data visualization. In *Proceedings of IEEE Visualization 2005*, pages 190–198. Available from: http://visit.llnl.gov/.

Cladouhos, T., Bekele, E., and Cahill, T. (1989). The November 25, 1988 Saguenay earthquake: Isoseismal survey in Ithaca region, central New York. *Seismological Research Letters*, 60(3):131–133. Available from: http://dx.doi.org/10.1785/gssrl.60.3.131.

GoldCorp (2001). US$575,000 goldcorp challenge awards world's first 6 million ounce internet gold rush yields high grade results! Press Release. Available from: http://www.infomine.com/index/pr/Pa065434.PDF.

Holom, D. I. and Oldow, J. S. (2007). Gravity reduction spreadsheet to calculate the bouguer anomaly using standardized methods and constants. *Geosphere*, 3(2):86+. Available from: http://dx.doi.org/10.1130/ges00060.1.

Hornby, P., Boschetti, F., and Horowitz, F. G. (1999). Analysis of potential field data in the wavelet domain. *Geophysical Journal International*, 137(1):175–196. Available from: http://dx.doi.org/10.1046/j.1365-246x.1999.00788.x.

Hornby, P., Horowitz, F. G., and Boschetti, F. (2002). A physical interpretation of the Poisson wavelet transform of potential fields. In *Proceedings, EGS XXVII General Assembly*, Munich. European Geophysical Society, European Geophysical Society. Available from: http://www.cosis.net/abstracts/EGS02/05568/EGS02-A-05568.pdf.

Horowitz, F. G. and Gaede, O. (2014). BSDWormer; an open source implementation of a Poisson wavelet multiscale analysis for potential fields. In *2014 Fall Meeting*, number T43C-4743. American Geophysical Union. Available from: http://abstractsearch.agu.org/meetings/2014/FM/T43C-4743.html.

Jessell, M. (2001). An atlas of structural geophysics II. *Journal of the Virtual Explorer*, 05. Available from: http://virtualexplorer.com.au/journal/2001/05.

Lebigot, E. O. (2018). Uncertainties: a Python package for calculations with uncertainties. Online. Available from: http://pythonhosted.org/uncertainties/.

Mallat, S. and Zhong, S. (1992). Characterization of signals from multiscale edges. *Pattern Analysis and Machine Intelligence, IEEE Transactions on*, 14(7):710–732. Available from: http://dx.doi.org/10.1109/34.142909.

Moreau, F., Gibert, D., Holschneider, M., and Saracco, G. (1997). Wavelet Analysis of Potential Fields. *Inverse Problems*, 13:165–178. Available from: http://dx.doi.org/10.1088/0266-5611/13/1/013.

Navarrete, L. (2015). Crustal structure of NE n. america from constrained models of potential field data. Master's thesis, University of Rochester.

Nettleton, L. L. (1939). Determination of density for reduction of gravimeter observations*. *GEOPHYSICS*, 4(3):176–183. Available from: http://dx.doi.org/10.1190/1.0403176.

Parasnis, D. S. (1952). A study of rock densities in the english midlands. *Geophysical Supplements to the Monthly Notices of the Royal Astronomical Society*, 6(5):252–271. Available from: http://dx.doi.org/10.1111/j.1365-246x.1952.tb03013.x.

Podwysocki, M. H., Pohn, H. A., Phillips, J. D., Krohn, M. D., Purdy, T. L., and Merin, I. S. (1982). Evaluation of remote sensing, geological and geophysical data for south-central New York and northern Pennsylvania. *USGS Open-File Report*, (82-319):179. Available from: http://dx.doi.org/10.3133/ofr82319.

Reid, A. B., Allsop, J. M., Granser, H., Millett, A. J., and Somerton, I. W. (1990). Magnetic interpretation in three dimensions using Euler deconvolution. *GEOPHYSICS*, 55(1):80–91. Available from: http://dx.doi.org/10.1190/1.1442774.

RungePincockMinarco (2015). Data Integration and 3d Visualisation Software - FRACSIS. webpage retrieved 23 June 2015. Available from: http://www.rpmglobal.com/mining-software/data-visualisation-fracsis.

Schroeder, W., Martin, K., and Lorensen, B. (2004). *The Visualization Toolkit*. Kitware Inc., third edition. Available from: http://www.amazon.com/exec/obidos/redirect?tag=citeulike07-20&path=ASIN/1930934122.

Stone & Webster Engineering Corporation, Battelle Memorial Institute, Office of Nuclear Waste Isolation, and United States Department of Energy (1978). *Regional Geology of the Salina Basin: Report of Geologic Project Manager – Salina Basin : Phase I, August 1977 - January 1978*. Stone & Webster Engineering Corporation. Available from: https://books.google.com/books?id=1scWtwAACAAJ.

Winester, D. (1993). Buffalo AA; Gravity Station Description. Available from: http://www.gis.utep.edu/subpages/states/documents/NewYork/buffalo%20aa.pdf.

Yamamoto, A. (1999). Estimating the optimum reduction density for gravity anomaly: A theoretical overview. *Journal of the Faculty of Science, Hokkaido University.*, 11(3):577–599. Available from: http://hdl.handle.net/2115/8850.

Acknowledgements

I thank Ming Khan, as well as Emily Boedo, Samantha Moruzzi, and Ole Gustafson for their able field assistance during the gravity measurement campaign of this project. I thank Muawia Barazangi for pointing out the Cladouhos et al. reference. I thank Cindy Ebinger for suggesting that seismic basin amplification might be responsible for my noisy gravity measurements in downtown Ithaca. I thank Allan Duchoslav, of Zebra Earth Sciences for assistance and advice on using the CG5 – and for his patience with the border crossing troubles the instrument had. I thank Mark Castner of Canisius College in Buffalo for his assistance with my measuring the BUFFALO AA absolute gravity site.